Applied Surface Science 505 (2020) 144620

Contents lists available at ScienceDirect

Applied Surface Science

journal homepage: www.elsevier.com/locate/apsusc

Full Length Article

High Curie temperature ferromagnetism in penta-MnN_2 monolayer

Kexian Zhao, Qian Wang*

Center for Applied Physics and Technology, Department of Materials Science and Engineering, HEDPS, BKL-MEMD, College of Engineering, Peking University, Beijing 100871, China

ARTICLE INFO

Keywords:
High-Curie-temperature
Ferromagnetism
Pentagon structure
Electronic structure
Strain engineering
N_2 dimer

ABSTRACT

Two-dimensional (2D) intrinsic ferromagnetic materials with high Curie temperature have attracted increasing research interest because of their potential applications in spintronics. Here, on the basis of first principles calculations combined with Monte Carlo simulation, we report a new 2D pentagon-based monolayer, penta-MnN_2, which is not only dynamically, mechanically and thermally stable, but also exhibits half-metallicity with a band-gap of 1.12 eV in spin-down channel. More interestingly, penta-MnN_2 displays a high Curie temperature T_C of 913 K that can be further improved to 956 K when the biaxial tensile strain of 3% is applied. Compared to the reported hexagonal MnN monolayer, the exchange interaction between the Mn atoms is significantly enhanced in the penta-MnN_2 sheet due to its unique geometric configuration composed solely of the pentagons containing N_2 dimers.

1. Introduction

Spintronics has received extensive attention in science and technology in the past decades because it provides a new approach for data storage and information transmission by exploiting the spin degree of freedom of electrons [1,2]. Mn atom, because of its special electronic configuration of $3d^5 4s^2$, has been widely used for the design of magnetic materials, especially for 2D ferromagnetic monolayers. For instance, it has been found that MnO_2 monolayer is an intrinsic ferromagnetic semiconductor with T_C of 140 K [3]. Mn phthalocyanine (MnPc) sheet is ferromagnetic with *Tc* of 150 K [4], and the ferromagnetic Curie temperature can be further tuned by chlorination [5] or by strain [6]. $Mn_3C_{12}S_{12}$ monolayer [7] is ferromagnetic with *Tc* of 212 K that can be modulated by replacing the sulfur atoms with the imino group (−NH−), the resulting $Mn_3C_{12}N_{12}H_{12}$ sheet exhibits strong ferromagnetism with *Tc* of 450 K [8]. MnS_2 and $MnSe_2$ monolayers are ferromagnetic with *Tc* of 225 and 250 K, respectively, which can be further enhanced to 330 K and 375 K by applying 5% biaxial tensile strains [9]. Very recently, a graphene-like hexagonal MnN monolayer, named Hex-MnN, was also found to be ferromagnetic with *Tc* about room temperature (368 K) [10].

The origin of ferromagnetism exhibiting in transition metal (TM)-based 2D materials has been explored [11–15]. It is believed that the ferromagnetic orders are generated by direct TM-TM exchange or super-exchange among TM and its ligands [16–19]. For the 2D ferromagnetic materials containing Mn atoms, the magnetic coupling between Mn atoms has been found to be sensitive to the Mn−Mn distance and geometric configurations. For example, in orthorhombic and monoclinic-layered $LiMnO_2$, the coupling between the two Mn atoms changes from ferromagnetic (FM) phase to antiferromagnetic (AFM) phase when the Mn−Mn distance is reduced from 2.82 to 2.79 Å [20], and AFM coupling on or near the surface of $Ga_{1-x}Mn_xN$ can be driven by Mn−Mn bond length contraction [21], and the magnetic coupling can switch for AFM to FM in bulk Mn [22]. It is such sensitivity of magnetic coupling between Mn atoms to the atomic distance and local bonding environment that make Mn-based materials display diverse magnetic properties with flexible controllability.

Here, we propose a new 2D monolayer composed exclusively of the pentagonal rings containing N_2 dimer, labeled penta-MnN_2, and systematically study its magnetic properties by using density functional theory (DFT) and Monte Carlo (MC) simulation. It is one counterpart of manganese nitride including Mn_4N_3, Mn_4N, Mn_3N_2, MnN, most of which have robust ferromagnetism [23–27]. We also show that, different from previously reported 2D Mn-containing monolayers, when going from hexagonal structural units to pentagonal ones, and from atomic N to dimer N_2, the Curie temperature T_C increases significantly from 368 K in Hex-MnN sheet [10] to 913 K in the penta-MnN_2 sheet.

2. Computational method

Structural and electronic properties are performed by using Vienna Ab initio Simulation Package (VASP) [28] based on DFT. The ion-

* Corresponding author.
E-mail address: qianwang2@pku.edu.cn (Q. Wang).

https://doi.org/10.1016/j.apsusc.2019.144620
Received 2 September 2019; Received in revised form 30 October 2019; Accepted 5 November 2019
Available online 18 November 2019
0169-4332/

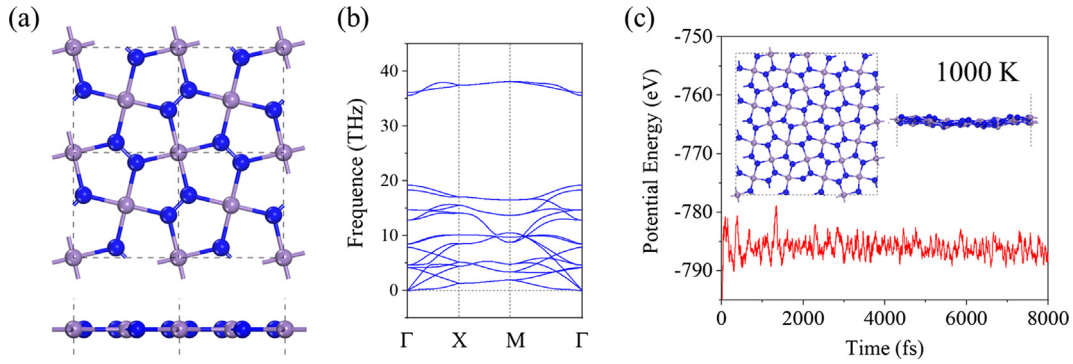

Fig. 1. (a) Top and side views of the optimized geometrical structure of penta-MnN_2, (b) phonon spectra, (c) variation of the total potential energy with simulation time during AIMD simulation at 1000 K. The insets are the top and side views of the geometrical structures in the end of simulation.

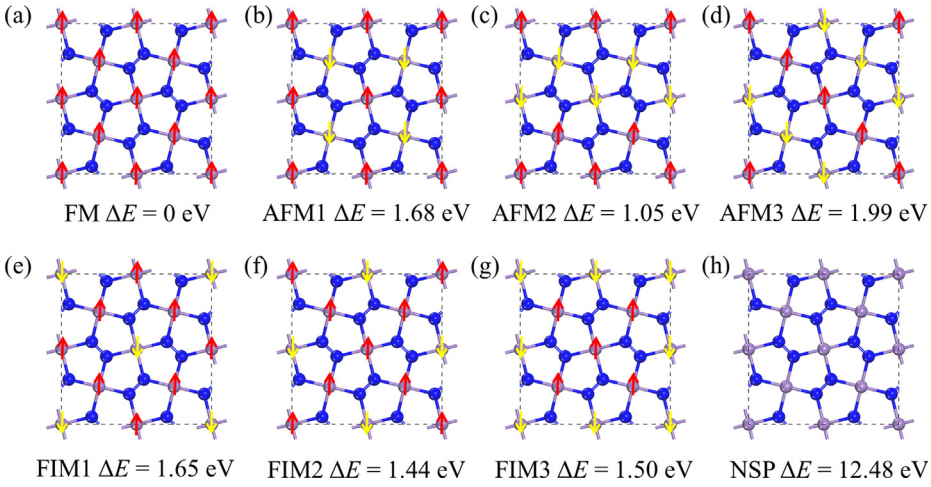

Fig. 2. Different spin coupling configurations for the penta-MnN_2 monolayer: (a) FM, (b) AFM1, (c) AFM2, (d) AFM3, (e) FIM1, (f) FIM2, (g) FIM3 and (h) NSP. Red and yellow arrows represent spin up and spin down states, respectively. (For interpretation of the references to color in this figure legend, the reader is referred to the web version of this article.)

electron interactions are treated with projector augmented wave potential (PAW) [29], and the exchange and correlation potential is described with the Perdew–Burke–Ernzerhof (PBE) functional. [30] Considering the strong correlated interaction of *d* electrons, the GGA + U method with U_{eff} = 4 eV is applied for the *d* orbitals of Mn atoms [31,32]. The convergence criteria for total energy and forces are set to be 10^{-4} eV and 10^{-2} eV/Å, respectively. Plane waves with a kinetic energy cutoff of 600 eV are used to expand the valence electron wave functions. The first Brillouin zone is sampled by using a 9 × 9 × 1 k-point grid within the Monkhorst–Pack scheme [33]. To confirm the dynamic stability, phonon spectra are calculated with PHONOPY package [34]. *Ab initio* molecular dynamics (AIMD) simulations are performed to confirm the thermal stability [35].

3. Results and discussion

The optimized structure of penta-MnN_2 monolayer is shown in Fig. 1(a), which is purely composed of the pentagons, belonging to the 2D pentagon-based structure family initiated by penta-graphene [36]. The side view shows that penta-MnN_2 has planar geometric configuration with *P4/mbm* symmetry (space group No. 127), similar to penta-PtN_2 and penta-PdN_2 [37]. The lattice parameters are found to be $a = b = 4.80$ Å with Mn−N bond length of 2.00 Å, N−N bond length of 1.30 Å, bond angles $\theta_{N\text{-}Mn\text{-}N} = 90^{\circ}$, $\theta_{Mn\text{-}N\text{-}Mn} = 118^{\circ}$and $\theta_{N\text{-}N\text{-}Mn} = 121^{\circ}$.

To verify the dynamic stability of penta-MnN_2 sheet, we calculate the phonon dispersion as shown in Fig. 1(b). The absence of imaginary modes in the entire Brillouin zone indicates that the penta-MnN_2 monolayer is dynamically stable. Then, the AIMD simulations are performed to further confirm the thermal stability. The 4 × 4 × 1 supercell is used in simulation for 8 picoseconds (*ps*) with a time step of 1 fs (*fs*) at 800, 1000 and 1200 K, respectively. The structure remains almost intact at 800 K, while it does not suffer from significant distortion at 1000 K, but the geometry breaks when the temperature is increased to 1200 K. The total potential energy only fluctuates slightly around constants at 800 and 1000 K. The simulation results at 1000 K are plotted in Fig. 1(c), showing that penta-MnN_2 has good thermal stability.

We then check the mechanical stability by calculating the linear elastic constant using the finite distortion method [38]. The calculated elastic constants are found to be $C_{11} = C_{22} = 116.10$ N/m, $C_{12} = 21.13$ N/m, $C_{44} = 31.48$ N/m, which meet Born-Huang criteria [39], namely, $C_{11}C_{12} - {C_{12}}^2 > 0$, $C_{44} > 0$, indicating that the penta-MnN_2 monolayer is mechanically stable. Moreover, using the formula $E = ({C_{11}}^2 - {C_{12}}^2)/C_{11}$, the in-plane Young modulus is found to be 112.25 N/m, which is comparable to that of MoS_2 monolayer (120 N/m), and significantly larger than that of germanene (42 N/m) and silicene (61 N/m) [40], suggesting that the penta-MnN_2 sheet is stable enough for avoiding the curling.

Next, we carry out calculations for the FM, AFM, ferrimagnetic (FIM) and non spin-polarized (NSP) states, in a total of 8 configurations, as shown in Fig. 2. We set the total energy of the FM configuration as 0 eV, and the energy difference are also given in Fig. 2. One can see that the FM state has the lowest energy and is the most energetically stable state among all the configurations. The large energy difference between the FM and AFM or the FM and FIM states indicates that penta-MnN_2 would have robust ferromagnetism. Our calculations show that the local magnetic moments are 3.6 μ_B on each Mn site and −0.3 μ_B on each N site, leading to a net magnetic moment of 6.0 μ_B per unit. The isosurface of the spin density ($\rho_\uparrow - \rho_\downarrow$) is plotted in Fig. 3(a), the yellow

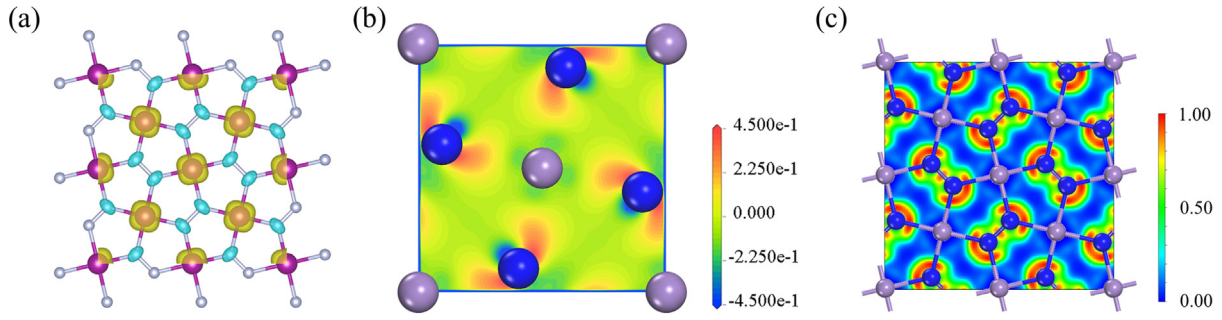

Fig. 3. (a) Spin-charge density (isosurfaces = 0.064 e/Å^{-3}), (b) deformation charge density and (c) ELF of penta-MnN_2.

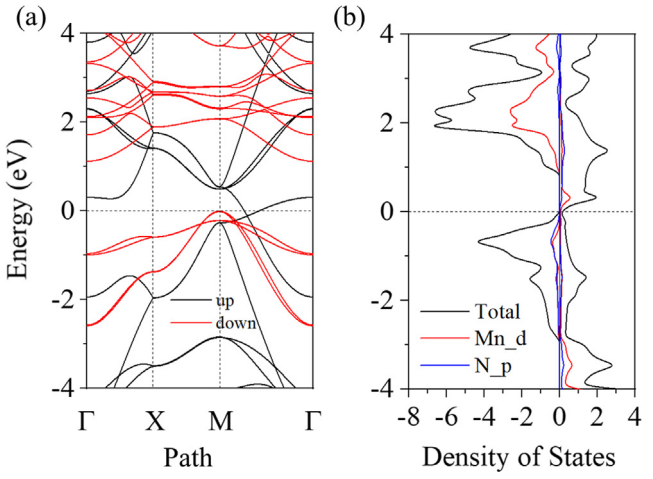

Fig. 4. (a) Spin-polarized band structures, and (b) the total and projected DOS of penta-MnN_2 using GGA + U (U_{eff} = 4 eV) method.

and blue regions represent the positive and negative values, respectively. It is obvious that the Mn atoms are highly spin-up polarized, while the N atoms are slightly spin-down polarized and antiferromagetically coupled with Mn, exhibiting the FM ordering between Mn atoms and weak AFM ordering between Mn and N atoms.

To study the charge distribution, we calculate the deformation charge density defined as the difference of charge density between the sheet and the corresponding isolated Mn and N atoms. The slice on the (0 0 1) plane is shown in Fig. 3(b), where the blue and red regions represent the depletion and accumulation of charge, respectively. One can see that the electrons transfer from Mn to N atom. Bader charge analysis [41–43] shows that each Mn atom transfers 1.36 *e* to each N_2 dimer. From the electron localization functions (ELF) slice on the (0 0 1) (Fig. 3(c)), it is obvious that the valence electrons are accumulated at N sites and partly localized on N—N bonds, showing covalent bond between N-N and ionic bond between Mn and N_2.

The spin-polarized electronic structures of the FM phase of penta-MnN_2 at GGA + U level are plotted in Fig. 4(a). One can see that penta-MnN_2 is an intrinsic ferromagnetic half-metal in which the spin-up bands cross the Fermi Level showing metal properties and the spin-down channel acts as a semiconductor with a gap of 1.12 eV, which is large enough to prevent the thermally excited spin-flip transition. Due to 100% spin polarization ratio near the Fermi level of half-metal, penta-MnN_2 shows good promise for spintronic devices.

To further understand the electronic structures and ferromagnetism behavior, the density of states (DOS) projected on atomic orbitals is calculated using GGA + U method, as plotted in Fig. 4(b), which indicates that penta-MnN_2 is half-metallic, the spin-up channel shows metallic characteristics whereas the spin-down channel is semiconducting. Furthermore, magnetism mainly comes from the contribution of *d* orbitals of Mn atoms and *p* orbitals of N atoms.

The electronic structure can further be tuned by applying strain ε defined as $(a - a_0)/a_0 \times 100\%$, where a_0 and a are the lattice constants of the penta-MnN_2 in its equilibrium and strained states, respectively. To simulate the real situation, we apply biaxial tensile strain ε from 0 to 5%. The band structures are recalculated to check if the half-metallicity can be preserved. As shown in Fig. 5, when the ε is changed from 0 to 5%, the conduction band minimum (CBM) of spin-down channel goes up and the valence band maximum (VBM) keeps nearly unchanged. However, the VBM of spin-down channel shifts up crossing the Fermi level, thus leading to metallicity when the biaxial strain is more than 3%. Namely, penta-MnN_2 remains ferromagnetic half-metallic when biaxial tensile strain is below 3%, and becomes ferromagnetic metal otherwise.

To evaluate the stability of ferromagnetic state, the Curie temperature (T_C) of penta-MnN_2 is calculated using Monte Carlo (MC) simulation based on Ising model, which has been extensively and successfully employed to evaluate the T_C of 2D FM materials [4,44–46]. The Hamiltonian of Ising model is defined as

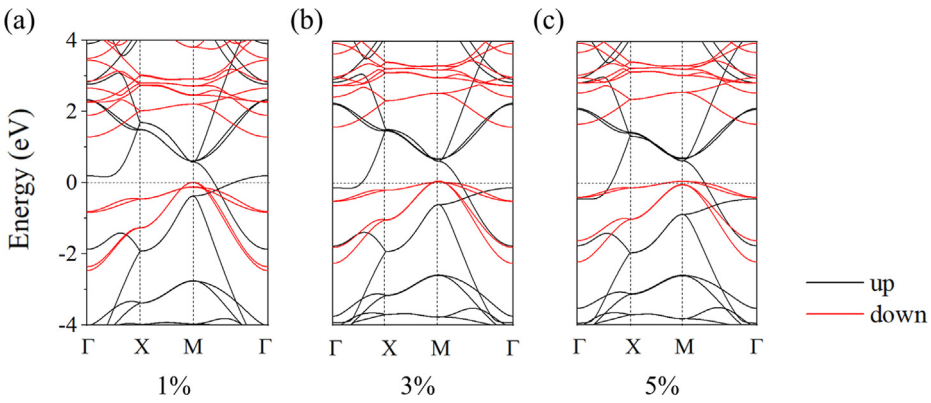

Fig. 5. Band structure of penta-MnN_2 under biaxial tensile strain of (a) 1%, (b) 3%, and (c) 5%.

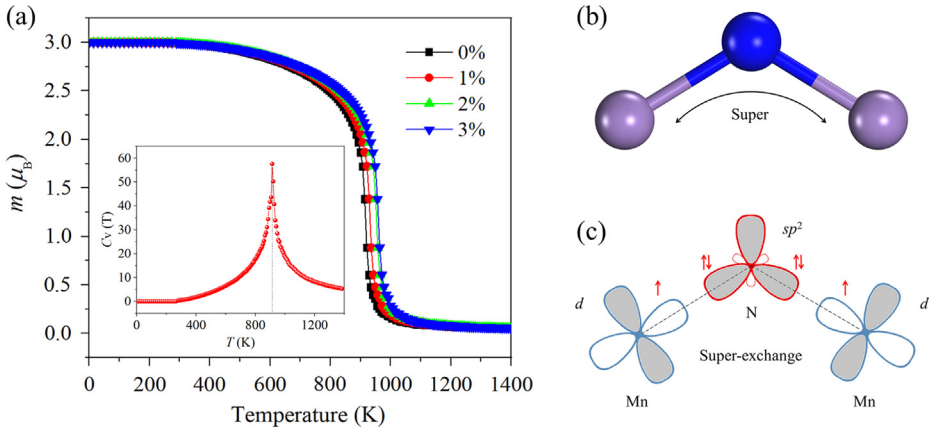

Fig. 6. (a) Variations of the magnetic moment of Mn with temperature under different biaxial tensile strain. The inset is specific heat (C_v) as a function of temperature without strain. (b) Schematic super-exchange (Mn—N_2—Mn) interaction. (c) Schematic description of the mechanism of super-exchange interaction for the Mn—N—Mn in penta-MnN_2.

Table 1
Results for different biaxial tensile strains.

Biaxial strain	m (μ_B)	E_{ex} (eV)	J (meV)	T_C (K)
0	3.0	0.430	5.972	913
1%	3.0	0.437	6.069	929
2%	3.0	0.447	6.208	950
3%	3.0	0.450	6.250	956

$$H = -\sum_{ij} J_{ij} M_i M_j$$

where J_{ij} represents the magnetic exchange coupling parameter between the two nearest-neighboring spins, M_i and M_j are the spin magnetic moment on i and j sites. In penta-MnN_2, M is 3.0 μ_B for Mn atoms. The exchange parameter J can be estimated from the exchange energy with the formula $J = E_{ex}/8M^2 = 5.97$ meV, where the exchange energy is defined as $E_{ex} = E_{AFM} - E_{FM}$, and $E_{AFM} = +4JM^2$, $E_{FM} = -4JM^2$. The MC simulation is implemented using an $80 \times 80 \times 1$ supercell to reduce the periodic constraints, and 5×10^9 steps are taken for each temperature. In our simulations, the spins on all magnetic sites flip randomly. Fig. 6(a) shows the variation of the magnetic moment with respect to temperature. The T_C of the penta-MnN_2 sheet is found to be 913 K, which is higher than most reported 2D materials [3,45–49] but comparable to that of MnP and MnAs monolayers [18]. When applying 3% biaxial tensile strain which can keep the half-metallicity of penta-MnN_2, the T_C increases to 956 K. The results are shown in Table 1.

The robust ferromagnetic coupling in penta-MnN_2 can be understood by the strong exchange interaction between the Mn atoms mediated by N_2. With an electronic configuration of half-filled 3*d* and filled 4*s* shells, Mn is unique in the 3*d* transition metal series. The coupling between the Mn atoms in Mn_2 dimer is antiferromagnetic, but becomes ferromagnetic when N is introduced [50]. In Hex-MnN monolayer [10], the Mn—N bond length is 1.956 Å, less than the value of 2.00 Å in penta-MnN_2, namely having a longer Mn—Mn bond length in our case, favorable to the FM coupling in penta-MnN_2 as discussed above. In addition, the super-exchange interaction between the Mn atoms is mediated through the N_2. According to the Good-enough–Kanamori–Anderson (GKA) rules [51–53], the super-exchange interaction usually favors ferromagnetic ordering, especially for the systems with a bond angle of 90° because the orbitals between the cation and anion are orthogonal. Although the angle of Mn—N—Mn is close to 120°, the orbitals of Mn and N are still orthogonal resulting from the fact that the N atoms form sp^2 hybrid orbitals, as shown in Fig. 6(c). From the Heitler–London model [54,55], the super-exchange integral J can be expressed as $J \approx 2k + 4\beta S$, where k is the exchange potential that is positive due to the Hund's rule, β and S are the hopping and overlap integral. The orthogonal orbitals lead to a negligible overlap integral S that is near zero, so that J is reduced to 2 k, which is positive. From the discussion above, the super-exchange interaction is positive, leading to the favorable FM ordering.

4. Conclusion

In summary, we have reported a robust intrinsic ferromagnetism in the penta-MnN_2 sheet composed of only pentagonal structural units, which is stable dynamically, thermally and mechanically. The ferromagnetism is mainly contributed by the Mn_*d* and N_*p* orbitals. The ferromagnetic ordering state is energetically more favorable than the antiferromagnetic one. The unique geometric configuration of the pentagon with N_2 dimer in penta-MnN_2 makes the system highly intriguing: exhibiting stable half-metallicity and robust ferromagnetism with a Curie temperature of 913 K, which is much higher than other reported Mn-containing 2D structures. Moreover, the T_C can be further increased to 956 K under 3% tensile strain. From the ferromagnetic transition in Mn_2 dimer mediated by N, to the room temperature ferromagnetism in the hexagonal MnN sheet, and to the high Curie temperature ferromagnetism in the pentagonal MnN_2 sheet, the displayed diversity of magnetism in Mn-based structures suggests that it is highly flexible to design new magnetic Mn-containing materials. The penta-MnN_2 sheet with the high T_C and half-metallicity has the potential for future spintronic applications with high performance.

Declaration of competing interest

The authors declare that they have no known competing financial interests or personal relationships that could have appeared to influence the work reported in this paper.

Acknowledgements

This work is partially supported by grants from the National Natural Science Foundation of China (Grants No. 21773004 and No. 11974028), the National Key Research and Development Program of the Ministry of Science and Technology of China (Grants No. 2017YFA0205003 and No. 2016YFE0127300), and is supported by the High Performance Computing Platform of Peking University, China.

References

[1] A. Fert, Nobel lecture: origin, development, and future of spintronics, Rev. Mod. Phys. 80 (2008) 1517–1530.
[2] X. Li, J. Yang, First-principles design of spintronics materials, Natl. Sci. Rev. 3 (2016) 365–381.
[3] M. Kan, J. Zhou, Q. Sun, Y. Kawazoe, P. Jena, The intrinsic ferromagnetism in a MnO_2 monolayer, J. Phys. Chem. Lett. 4 (2013) 3382–3386.
[4] J. Zhou, Q. Sun, Magnetism of phthalocyanine-based organometallic single porous sheet, J. Am. Chem. Soc. 133 (2011) 15113–15119.

[5] J. Zhou, Q. Sun, Absorption induced modulation of magnetism in two-dimensional metal-phthalocyanine porous sheets, J. Chem. Phys. 138 (2013) 204706.
[6] J. Zhou, Q. Wang, Q. Sun, Y. Kawazoe, P. Jena, Strain-induced spin crossover in phthalocyanine-based organometallic sheets, J. Phys. Chem. Lett. 3 (2012) 3109–3114.
[7] M. Zhao, A. Wang, X. Zhang, Half-metallicity of a kagome spin lattice: the case of a manganese bis-dithiolene monolayer, Nanoscale 5 (2013) 10404–10408.
[8] J. Liu, Q. Sun, Enhanced ferromagnetism in a $Mn_3C_{12}N_{12}H_{12}$ sheet, Chem. Phys. Chem. 16 (2015) 614–620.
[9] M. Kan, S. Adhikari, Q. Sun, Ferromagnetism in MnX_2 (X = S, Se) monolayers, Phys. Chem. Chem. Phys. 16 (2014) 4990–4994.
[10] Z. Xu, H. Zhu, Two-dimensional manganese nitride monolayer with room temperature rigid ferromagnetism under strain, J. Phys. Chem. C 122 (2018) 14918–14927.
[11] A. Avsar, A. Ciarrocchi, M. Pizzochero, D. Unuchek, O.V. Yazyev, A. Kis, Defect induced, layer-modulated magnetism in ultrathin metallic $PtSe_2$, Nat. Nanotechnol. 14 (2019) 674–678.
[12] C. Huang, J. Feng, F. Wu, D. Ahmed, B. Huang, H. Xiang, K. Deng, E. Kan, Toward intrinsic room-temperature ferromagnetism in two-dimensional semiconductors, J. Am. Chem. Soc. 140 (2018) 11519–11525.
[13] X. Li, J. Yang, Toward room-temperature magnetic semiconductors in two-dimensional ferrimagnetic organometallic lattices, J. Phys. Chem. Lett. 10 (2019) 2439–2444.
[14] L. Shen, R.Q. Wu, H. Pan, G.W. Peng, M. Yang, Z.D. Sha, Y.P. Feng, Mechanism of ferromagnetism in nitrogen-doped ZnO: first-principle calculations, Phys. Rev. B 78 (2018) 073306.
[15] J. Zhou, Q. Wang, Q. Sun, P. Jena, Electronic and magnetic properties of a BN sheet decorated with hydrogen and fluorine, Phys. Rev. B 81 (2010) 085442.
[16] V.V. Kulish, W. Huang, Single-layer metal halides MX_2 (X = Cl, Br, I): stability and tunable magnetism from first principles and Monte Carlo simulations, J. Mater. Chem. C 5 (2017) 8734–8741.
[17] B. Wang, Q. Wu, Y. Zhang, Y. Guo, X. Zhang, Q. Zhou, S. Dong, J. Wang, High Curie-temperature intrinsic ferromagnetism and hole doping-induced half-metallicity in two-dimensional scandium chlorine monolayers, Nanoscale Horiz. 3 (2018) 551–555.
[18] B. Wang, Y. Zhang, L. Ma, Q. Wu, Y. Guo, X. Zhang, J. Wang, MnX (X= P, As) monolayers: a new type of two-dimensional intrinsic room temperature ferromagnetic half-metallic material with large magnetic anisotropy, Nanoscale 11 (2019) 4204–4209.
[19] X. Zhang, B. Wang, Y. Guo, Y. Zhang, Y. Chen, J. Wang, High Curie temperature and intrinsic ferromagnetic half-metallicity in two-dimensional Cr_3X_4 (X = S, Se, Te) nanosheets, Nanoscale Horiz. 4 (2019) 859–866.
[20] G. Ceder, S.K. Mishra, The stability of orthorhombic and monoclinic-layered $LiMnO_2$, Electrochem. Solid-State Lett. 2 (1999) 550–552.
[21] Q. Wang, Q. Sun, P. Jena, Y. Kawazoe, Antiferromagnetic coupling driven by bond length contraction near the $Ga_{1-x}Mn_xN$ film surface, Phys. Rev. Lett. 93 (2004) 155501.
[22] D. Hobbs, J. Hafner, D. Spišák, Understanding the complex metallic element Mn. I. Crystalline and noncollinear magnetic structure of α-Mn, Phys. Rev. B 68 (2003) 014407.
[23] J. Guerrero-Sánchez, A.-O. Mandru, K. Wang, N. Takeuchi, G.H. Cocoletzi, A.R. Smith, Structural, electronic and magnetic properties of Mn_3N_2 (0 0 1) surfaces, Appl. Surf. Sci. 355 (2015) 623–630.
[24] J. Guerrero-Sánchez, N. Takeuchi, Structural stability and the electronic and magnetic properties of ferrimagnetic Mn_4N (0 0 1) surfaces, Appl. Surf. Sci. 407 (2017) 209–212.
[25] K. Inumaru, T. Nishikawa, K. Nakamura, S. Yamanaka, High-pressure synthesis of superconducting molybdenum nitride δ-MoN by in situ nitridation, Chem. Mater. 20 (2008) 4756–4761.
[26] H. Yang, R. Yang, A.R. Smith, W.R.L. Lambrecht, Atomic-scale structure of g-phase Mn_3N_2 (0 1 0) studied by scanning tunneling microscopy and first-principles theory, Surf. Sci. 548 (2004) 117–128.
[27] R. Yu, X. Chong, Y. Jiang, R. Zhou, W. Yuan, J. Feng, The stability, electronic structure, elastic and metallic properties of manganese nitrides, Rsc Adv. 5 (2015) 1620–1627.
[28] G. Kresse, J. Furthmuller, Efficient iterative schemes for ab initio total-energy calculations using a plane-wave basis set, Phys. Rev. B 54 (1996) 11169–11186.
[29] P.E. Blochl, Projector augmented-wave method, Phys. Rev. B 50 (1994) 17953–17979.
[30] J.P. Perdew, K. Burke, M. Ernzerhof, Generalized gradient approximation made simple, Phys. Rev. Lett. 77 (1996) 3865–3868.
[31] J. Heyd, G.E. Scuseria, M. Ernzerhof, Hybrid functionals based on a screened Coulomb potential, J. Chem. Phys. 118 (2003) 8207–8215.
[32] W. Setyawan, R.M. Gaume, S. Lam, R.S. Feigelson, S. Curtarolo, High-throughput combinatorial database of electronic band structures for inorganic scintillator materials, ACS Comb. Sci. 13 (2011) 382–390.
[33] H.J. Monkhorst, J.D. Pack, Special points for Brillouin-zone integrations, Phys. Rev. B 13 (1976) 5188–5192.
[34] A. Togo, F. Oba, I. Tanaka, First-principles calculations of the ferroelastic transition between rutile-type and $CaCl_2$-type SiO_2 at high pressures, Phys. Rev. B 78 (2008) 134106.
[35] D. Bucher, L.C. Pierce, J.A. McCammon, P.R. Markwick, On the use of accelerated molecular dynamics to enhance configurational sampling in ab initio simulations, J. Chem. Theory Comput. 7 (2011) 890–897.
[36] S.H. Zhang, J. Zhou, Q. Wang, X.S. Chen, Y. Kawazoe, P. Jena, Penta-graphene: a new carbon allotrope, P. Natl. Acad. Sci. USA 112 (2015) 2372–2377.
[37] K. Zhao, X. Li, S. Wang, Q. Wang, 2D planar penta-MN_2 (M = Pd, Pt) sheets identified through structure search, Phys. Chem. Chem. Phys. 21 (2018) 246–251.
[38] Y. Le Page, P. Saxe, Symmetry-general least-squares extraction of elastic data for strained materials from ab initio calculations of stress, Phys. Rev. B 65 (2002) 104104.
[39] J. Wang, S. Yip, S.R. Phillpot, D. Wolf, Crystal instabilities at finite strain, Phys. Rev. Lett. 71 (1993) 4182–4185.
[40] Q. Peng, S. De, Outstanding mechanical properties of monolayer MoS_2 and its application in elastic energy storage, Phys. Chem. Chem. Phys. 15 (2013) 19427–19437.
[41] G. Henkelman, A. Arnaldsson, H. Jónsson, A fast and robust algorithm for Bader decomposition of charge density, Comput. Mater. Sci. 36 (2006) 354–360.
[42] E. Sanville, S.D. Kenny, R. Smith, G. Henkelman, Improved grid-based algorithm for Bader charge allocation, J. Comput. Chem. 28 (2007) 899–908.
[43] W. Tang, E. Sanville, G. Henkelman, A grid-based Bader analysis algorithm without lattice bias, J. Phys.: Conden. Matt. 21 (2009) 084204.
[44] X. Li, X. Wu, J. Yang, Half-metallicity in $MnPSe_3$ exfoliated nanosheet with carrier doping, J. Am. Chem. Soc. 136 (2014) 11065–11069.
[45] J. Liu, Q. Sun, Y. Kawazoe, P. Jena, Exfoliating biocompatible ferromagnetic Cr-trihalide monolayers, Phys. Chem. Chem. Phys. 18 (2016) 8777–8784.
[46] Y. Sun, Z. Zhuo, X. Wu, J. Yang, Room-temperature ferromagnetism in two-dimensional Fe_2Si nanosheet with enhanced spin-polarization ratio, Nano Lett. 17 (2017) 2771–2777.
[47] C. Gong, L. Li, Z. Li, H. Ji, A. Stern, Y. Xia, T. Cao, W. Bao, C. Wang, Y. Wang, Z.Q. Qiu, R.J. Cava, S.G. Louie, J. Xia, X. Zhang, Discovery of intrinsic ferromagnetism in two-dimensional van der Waals crystals, Nature 546 (2017) 265–269.
[48] B. Huang, G. Clark, E. Navarro-Moratalla, D.R. Klein, R. Cheng, K.L. Seyler, D. Zhong, E. Schmidgall, M.A. McGuire, D.H. Cobden, W. Yao, D. Xiao, P. Jarillo-Herrero, X. Xu, Layer-dependent ferromagnetism in a van der Waals crystal down to the monolayer limit, Nature 546 (2017) 270–273.
[49] F. Wu, C. Huang, H. Wu, C. Lee, K. Deng, E. Kan, P. Jena, Atomically thin transition-metal dinitrides: high-temperature ferromagnetism and half-metallicity, Nano Lett. 15 (2015) 8277–8281.
[50] B.K. Rao, P. Jena, Giant magnetic moments of nitrogen-doped Mn clusters and their relevance to ferromagnetism in Mn-doped GaN, Phys. Rev. Lett. 89 (2012) 185504.
[51] P.W. Anderson, New approach to the theory of superexchange interactions, Phys. Rev. 115 (1959) 2–13.
[52] J.B. Goodenough, Theory of the role of covalence in the perovskite-type manganites [La, *M*(II)]MnO_3, Phys. Rev. 100 (1955) 564–573.
[53] T. Moriya, Anisotropic superexchange interaction and weak ferromagnetism, Phys. Rev. 120 (1960) 91–98.
[54] W. Heitler, F. London, Wechselwirkung neutraler atome und homöopolare bindung nach der quantenmechanik, Z. Phys. 44 (1927) 455–472.
[55] J.P. Launay, M. Verdaguer, Electrons in Molecules: From Basic Principles to Molecular Electronics, first ed., Oxford University Press, New York, 2013.